J Fluoresc (2017) 27:755–766
DOI 10.1007/s10895-016-2008-8

ORIGINAL ARTICLE

Nonlinear Interactions of Zinc Phthalocyanine-Graphene Quantum Dots Nanocomposites: Investigation of Effects of Surface Functionalization with Heteroatoms

Owolabi M. Bankole[1] · **Ojodomo J. Achadu**[1] · **Tebello Nyokong**[1]

Received: 26 October 2016 / Accepted: 20 December 2016 / Published online: 4 January 2017

Abstract This study reports the development of functional optical limiting materials composed of pristine graphene (GQDs), nitrogen-doped (NGQDs) and sulfur-nitrogen co-doped (SNGQDs) graphene quantum dots covalently linked to mono-amino substituted zinc phthalocyanine (**Pc**). Open aperture Z-scan technique was employed to monitor the behaviour of the conjugates under tightly focussed Gaussian laser beam using a mode-locked Nd:YAG laser delivering 10 nanosecond (FWHM) pulses at 532 nm wavelength. Nonlinear effect due to reverse saturable absorption was the predominant mechanism; and was attributed to the moderately enhanced triplet population. The major factor(s) responsible for the enhanced nonlinearities in the **Pc**-NGQDs and **Pc**-SNGQDs was fully described and attributed to the surface defects caused by the presence of heteroatoms of N and S.

Keywords Phthalocyanine · Graphene quantum dots · Nonlinear optics · 3rd order susceptibility · Hyperpolarizability

Introduction

Graphene quantum dots (GQDs) are zero-dimensional member of carbon-based nanomaterial family that have attracted tremendous attentions due to their unique electronic, optical, thermal, mechanical, and chemical properties [1–6]. New or improved intrinsic properties of pristine GQDs can be achieved by selective surface functionalization with heteroatoms such as nitrogen and sulfur [7, 8]. Pristine GQDs and their doped analogues have contributed to state-of-the-art technological applications such as photo-catalysis, bio-imaging, fuel cells and optical switches [4, 6, 8–12].

Recent applications of GQDs in optical switching is encouraging [11, 12], and may inspire the development of novel functional optical limiting (OL) materials to act as a shield for light sensitive materials from intense laser radiation. Recently, Bourlinos and co-workers reported on enhanced nonlinear absorption of nitrogeneuos boron doped carbon dots using 532 nm laser excitation [13]. The doping of GQDs with heteroatoms could encourage formation of new electronic states which can result in the enhancement of nonlinear optical (NLO) response of the nanomaterials [13, 14].

Unlike graphene quantum dots, optical limiting activities of metallophthalocyanines (MPcs) and their derivatives have been studied extensively. Their nonlinear effects are attributed to reverse saturable absorption as the dominant mechanism. Research efforts have been intensified lately to improve nonlinear optical properties of phthalocyanines and their derivatives in the presence of carbon-based materials such as fullerene [15], carbon nanotubes [16, 17] and graphene oxides [18]. NLO behaviour of MPcs in the presence of graphene quantum dots has not been reported, hence the aim of this work. The combination of GQDs and MPcs may result in improved NLO behavior through synergy since both are NLO materials.

Encouraged by the improved NLO responses of phthalocyanines in presence of carbon-nanostructures as mentioned above, herein, we present the studies on photophysical and NLO behavior of 2(3),9(10),16(17)-trikis-(4-*tert*-butylphenoxyl)-4-aminophthalocyaninato zinc (II) (represented as **Pc** throughout the manuscript), when covalently linked to pristine (GQDs), N-doped (NGQDs) and S, N co-doped (SNGQDs) graphene quantum dots. The **Pc** in this work

✉ Tebello Nyokong
t.nyokong@ru.ac.za

[1] Department of Chemistry, Rhodes University, Grahamstown 6140, South Africa

contains an amino group for linking to COOH groups of the respective graphene QDs. The *tert*-butyl substituents enabled solubility and reduced aggregation. We employed un-doped and doped GQDs linked to phthalocyanine to enable us compare the effects of doping of GQDs (with heteroatoms) on the NLO behavior of the **Pc**. NLO characterizations of the nanocomposites of the QDs covalently linked to phthalocyanine were evaluated using open aperture (OA) Z-scan technique.

Experimental

Materials

N N-dimethylformamide (DMF) and dimethyl sulphoxide (DMSO) were purchased from Merck. N-hydroxysuccinimide (NHS) and N-(3-dimethylaminopropyl)-N-ethylcarbodiimide hydrochloride (EDC) were purchased from Fluka. 2(3),9(10),16(17)-Trikis-(4-*tert*-butylphenoxyl)-4-aminophthalocyaninato zinc (II) (represented as **Pc**) was synthesized and purified according to the reported procedure [19, 20]. Pristine (GQDs), N-doped (NGQDs) and S, N co-doped (SNGQDs) graphene quantum dots were synthesized as we recently reported [21]. Ultra-pure water was obtained from a Mili-Q Water system (Millipore Corp. Bedford, MA, USA). All solvents used were of analytical reagent grade and were freshly distilled before use.

Equipment and Methods

Infra-red spectra were measured on a Bruker ALPHA FT-IR Spectrometer with universal attenuated total reflectance (ATR) sampling accessory. Ground state electronic absorption spectra were recorded on a Shimadzu UV-2550 spectrophotometer. Fluorescence emission spectra were recorded on a Varian Eclipse spectrofluorimeter. Time Correlated Single Photon Counting (TCSPC) setup (FluoTime 200, Picoquant GmbH) was used for the fluorescence decay studies. The excitation source was a diode laser (LDH-P-670 driven by PDL 800-B, 670 nm, 20 MHz repetition rate, 44 ps pulse width, Picoquant GmbH) for excitation where the Pc absorbs, and diode laser (LDH-P-485 with 10 MHz repetition rate, 88 ps pulse width, where GQDs absorb.

Transmission electron microscope (TEM) images were obtained using a JEOL TEM 1210 transmission electron microscope at 100 kV accelerating voltage. TEM samples were prepared by placing a drop of conjugates or quantum dots solution on the sample grid and allowing it to dry before measurements. X-ray powder diffraction patterns were recorded on a Bruker D8 Discover equipped with a LynxEye detector, using CuKα radiation ($\lambda = 1.5405$ Å, nickel filter). Details have been provided before [22].

X-ray photoelectron spectroscopy (XPS) analysis was done using an AXIS Ultra DLD, with Al (monochromatic) anode equipped with a charge neutraliser, supplied by Kratos Analytical as described before [22].

All Z-scan analyses were performed using a frequency-doubled Nd:YAG laser (Quanta-Ray, 1.5 J/10 ns fwhm pulse duration) as the excitation source. The laser was operated in a near Gaussian transverse mode at 532 nm (second harmonic), with a pulse repetition rate of 10 Hz and energy range of 0.1 μJ – 0.1 mJ, as limited by the energy detectors (Coherent J5-09), details have been provided before [23].

The nanosecond laser flash photolysis set-up used to investigate the triplet state behaviors, comprised of coupled laser systems, a Nd-YAG laser (already described above) pumping Lambda-Physik FL3002 dye (Pyridin 1 dye in methanol) laser [22].

Preparation of Pc-GQDs, Pc-NGQDs and Pc-SNGQDs (Scheme 1)

Covalent linking between the GQDs and the phthalocyanine was carried out using EDC /NHS coupling reactions. Briefly, 50 mg of GQDs, NGQDs or SNGQDs were separately dissolved in a vial containing 3 mL Millipore water. EDC (20 mg, 0.10 mmol) and NHS (15 mg, 0.13 mmol) were added to each of the QDs solution followed by stirring at room temperature for 24 h to activate the carboxylic groups (−COOH) of the GQDs. Then, 10 mg (9.63×10^{-6} mol) of the **Pc** in 3 mL DMF was added to each GQDs solution and the mixture stirred for another 24 h while monitoring the amide bond formation by FTIR. The resulting crude products were precipitated with dry absolute ethanol, and centrifuged several times to obtain the pure conjugates as the residues. The pure conjugates were oven-dried at 60 °C and denoted as **Pc**-GQDs, **Pc**-NGQDs and **Pc**-SNGQDs.

Photophysical Parameters

Fluorescence (Φ_F) and triplet (Φ_T) quantum yields of the **Pc** has been reported in the literature [23]. Φ_F and Φ_T of the **Pc** in presence of GQDs were determined in DMSO using comparative methods reported in the literature [24–27]. Unsubstituted ZnPc in DMSO, $\Phi_F = 0.2$ [24] and $\Phi_T = 0.65$ [25] was used as standard for fluorescence and triplet quantum yields. For excitation where the Pc absorbs, fluorescence quantum yield is represented as $\Phi_{F(Pc)}$.

Fluorescence quantum yields ($\Phi_{F(QDs)}$) for the GQDs, NGQDs or SNGQDs in aqueous solution have been reported before [21]. The fluorescence quantum yields of GQDs covalently linked to **Pc** ($\Phi_{F(Pc-QDs)}$) were estimated using Eq. (1):

$$\Phi_{F(Pc-QDs)} = \Phi_{F(QDs)} \frac{F_{(Pc-QDs)}}{F_{QDs}} \quad (1)$$

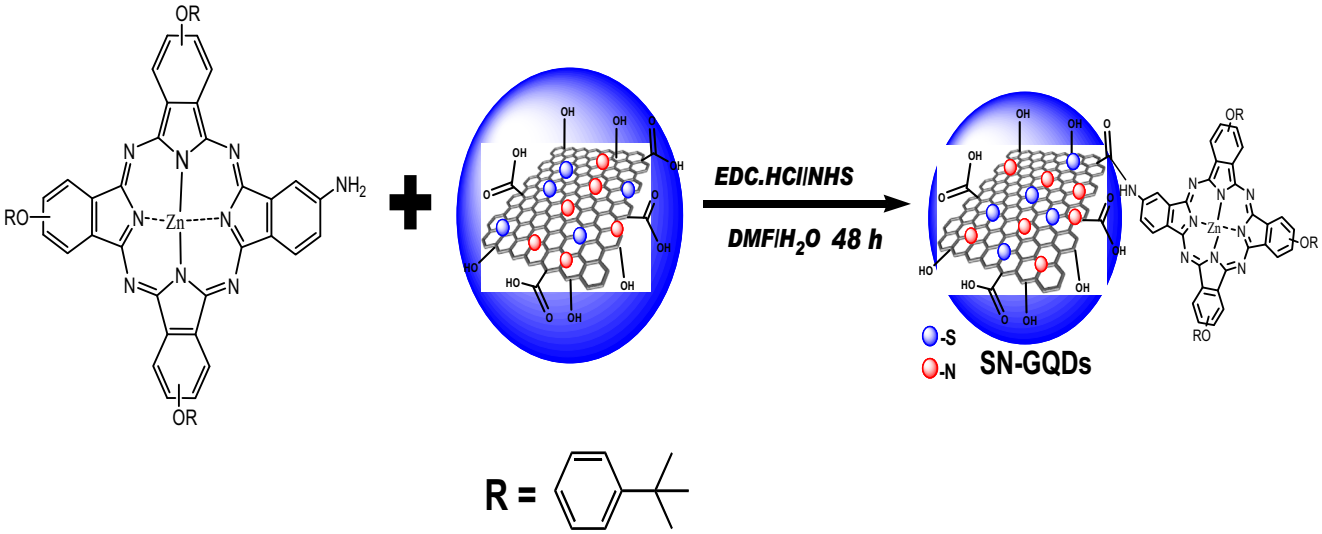

Scheme 1 Schematic representation of the covalent linking of graphene quantum dots S, N co-doped graphene (SNGQDs) quantum dots to zinc phthalocyanine (**Pc**)

where $F_{(Pc-QDs)}$ and F_{QDs} are the fluorescence intensities of GQDs in **Pc**-GQDs conjugates and quantum dots alone, respectively. $\Phi_{F(QDs)}$ represents the fluorescence quantum yield of the QDs alone and was used as a standard.

Nonlinear Optical Characterizations

Nonlinear interactions of the **Pc** conjugated to the graphene QDs under tightly focused Gaussian laser beam were evaluated with open-aperture (OA) Z-scan technique reported elsewhere [28, 29]. The technique is based on the measured transmittances as a function of the sample position z when samples are illuminated by nanosecond or femtosecond pulsed-laser systems. The magnitude of normalized transmittances (T(z)) as a function of sample position (z) relative to the focus (z = 0); and the nonlinear absorption coefficient, β_{eff}, can be calculated using Eq. (2), [30].

$$T(z) = \frac{1}{1 + \beta_{eff} L_{eff} \left(I_{00} \Big/ \left(1 + \left(z \Big/ z_0 \right)^2 \right) \right)} \tag{2}$$

where I_{00} is the intensity of the light on focus, β_{eff} is the effective nonlinear absorption coefficient, z_0 is the diffraction length of the beam, z is the sample position with respect to input intensity, L_{eff} is the effective length, respectively. L_{eff} in the sample of length L is defined in terms of the linear absorption coefficient, α, in Eq. 3:

$$L_{eff} = \frac{1 - e^{-\alpha L}}{\alpha} \tag{3}$$

A simpler numerical form of Eq. (2) which is well suited to fit the experimental data directly was employed, Eq. 4:

$$T(Z) = 0.363e^{\frac{-q(z)}{5.60}} + 0.286e^{\frac{-q(z)}{1.21}} + 0.213e^{\frac{-q(z)}{24.62}} + 0.096e^{\frac{-q(z)}{115.95}} + 0.038e^{\frac{-q(z)}{965.08}} \tag{4}$$

q(z) is calculated using Eq. 5:

$$q(z) = \frac{\beta_{eff} L_{eff} I_{00}}{1 + \left(z \Big/ z_0 \right)^2} \tag{5}$$

The imaginary part of the third-order susceptibility ($\mathrm{I_m}[\chi^{(3)}]$) is related to the nonlinear absorption coefficient, β_{eff}, and can be calculated using Eq. 6 [31]:

$$\mathrm{I_m}\left[\chi^{(3)}\right] = n^2 \varepsilon_0 c^2 \lambda \beta_{eff} \Big/ 4\pi^2 \tag{6}$$

where, n and c are the linear refractive index ($n = 1.479$ for DMSO), and speed of light respectively. ε_0 is the permittivity of free space and λ is the wavelength of the laser.

The relationship between second order hyperpolarizability (γ) and imaginary third-order susceptibility ($I_m[\chi^{(3)}]$) of the samples is expressed in equation Eq. 7 [31]:

$$\gamma = \frac{\mathrm{I_m}\left[\chi^{(3)}\right]}{f^4 C_{\mathrm{mol}} N_A} \tag{7}$$

where C_{mol} is the molar concentration of the active species in the triplet state, f is the Lorentz local field enhancement factor defined as $f = (n^2 + 2)/3$; n is the refractive index of the sample and N_A is the Avogadro constant.

Results and Discussions

Characterization of the Conjugates

The -COOH groups on the GQDs were converted to active COO^- via EDC/NHS mediated coupling reaction, and linked to amino group of the phthalocyanine (Scheme 1) to form amide bonds between the **Pc** and the GQDs. Depending on orientation, π-π interaction is also possible between the **Pc** and the GQDs. The conjugates obtained were purified and characterized by FT-IR, UV–vis, TEM, XRD and EDX.

FTIR Spectra

The surface functional groups on the QDs as well as the amide bonding to the **Pc** were verified by the FTIR spectra as shown in

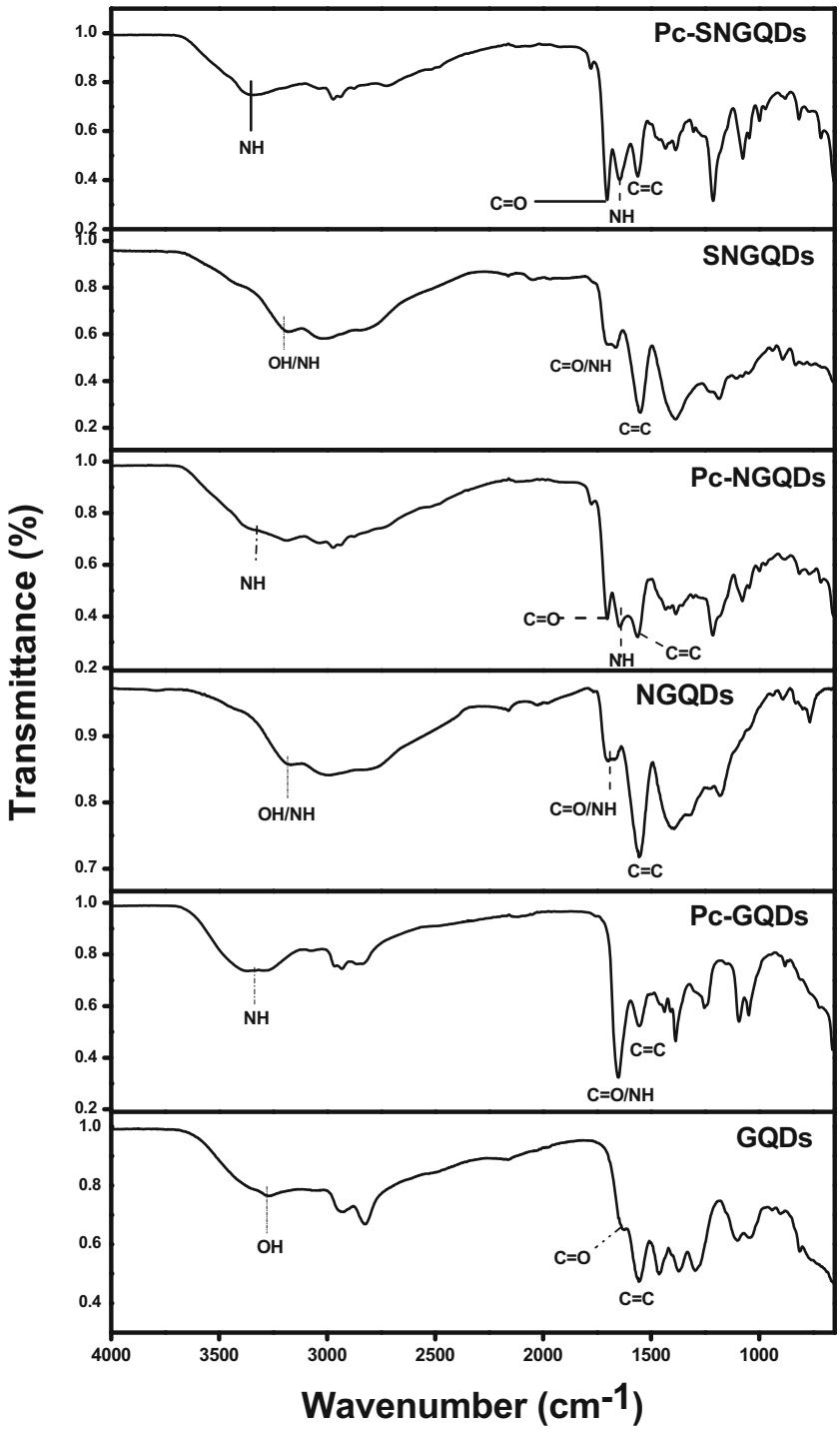

Fig. 1 FT-IR spectra of pristine GQDs, **Pc**-GQDs, NGQDS, **Pc**-NGQDs and SNGQDs and **Pc**-SNGQDs

Fig. 1. FTIR spectrum of pristine GQDs shows characteristic OH peak around 3400 cm^{-1} which is due to COOH on the surface of GQDs. For NGQDs and SNGQDs, the broad characteristic peaks due to OH/NH stretch around 2930–3400 cm^{-1} confirmed the presence of hydroxyl and secondary amine functional groups which co-existed on the surface of NGQDs and SNGQDs. These stretching vibrations of OH/NH were complemented by the presence of overlapped peaks of C = O (~1705 cm^{-1}), and NH (~1654 cm^{-1}) bending vibration due to COOH and CONH, respectively, for NGQDs and SNGQDs. FTIR spectra of the conjugates (**Pc**-GQDs, **Pc**-NGQDs and **Pc**-SNGQDs) revealed intense characteristics bands at ~ 1702 cm^{-1}, ~1647 cm^{-1} and 3340 cm^{-1} that are attributable to the amide vibrational bands of C = O, NH bending and NH stretch, respectively. The shift in the vibrational modes of OH and/or NH and C = O positions before and after covalent linking confirmed covalent interactions between the amine of phthalocyanine and carboxylic QDs.

XRD Data

The X-ray diffraction patterns of the as-prepared quantum dots and their phthalocyanine-QDs conjugates are shown in Fig. 2. The diffraction patterns of the graphene quantum dots (GQDs, NGQDS and SNGQDs) between 2 = 15° and 31°, corresponds to the graphitic structure [32, 33]. The broadness of the diffraction peaks is an indication of the small size of the quantum dots. Like graphene quantum dots, the broad peak observed for phthalocyanine positioned between 2 = 18° and

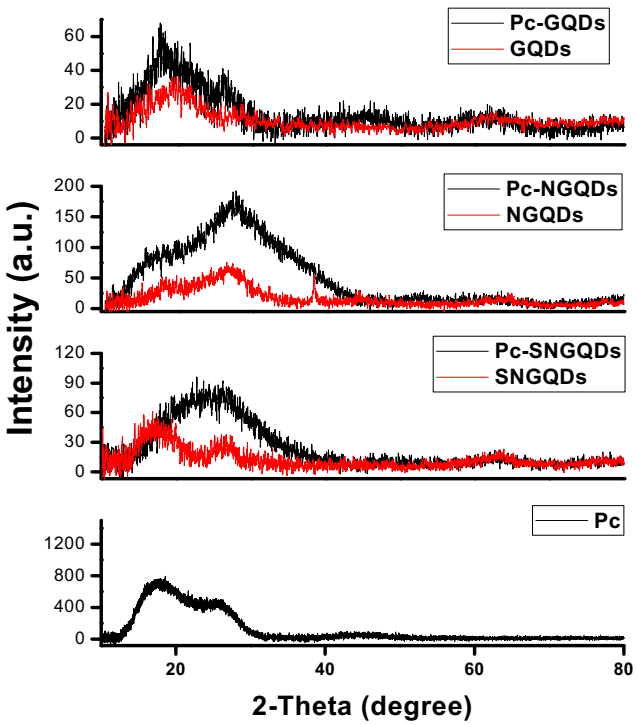

Fig. 2 X-ray diffraction patterns of **Pc**, SNGQDs, **Pc**-SNGQDs, NGQDs, **Pc**-NGQDs, GQDs and **Pc**-GQDs

27° is close to the 002 reflection plane of carbon which is the major constituent of phthalocyanines and QDs [34]. Conjugation of the **Pc** to QDs resulted in slightly sharper peaks suggesting possible increase in the size of the conjugates which could arise due to π-π stacking layers of the conjugates. Also, a noticeable reduction in the intensity of diffraction of **Pc** following conjugation to the graphene quantum dots is an indication of successful covalent interaction between the **Pc** and QDs.

TEM Images

Transmission electron microscopy (TEM) micrographs showed that the as-prepared GQDs are monodispersed with fairly spherical morphology and average particle size of ~ 3 nm, Fig. 3. The large interparticle distances prevent aggregation of the nanoparticles. The conjugation of the GQDs to the phthalocyanines resulted in the formation of clusters due to interaction of neighboring nanoparticles. Aggregation of graphene quantum dots in presence of phthalocyanine can also arise due to π–π stacking interaction of the aromatic ring of the phthalocyanine with the graphene QDs.

UV–Vis Spectra

Figure 4a shows the UV-visible absorption and photoluminescence (PL) spectra of the as-prepared graphene QDs recorded in water. Absorption bands were observed at 334 nm for GQDs and 341 nm for NGQDs. SNGQDs showed distinct absorption peak around 337 nm in addition to two other peaks positioned at 408 nm and 598 nm [8]. The PL excitation spectra of NGQDs and SNGQDs were slightly red-shifted compared to pristine GQDs due to the changes in chemical functionalities and defects on the graphene lattice by the heteroatoms [35]. The emission peaks of the GQDs were well resolved.

The absorption spectra of the **Pc** and when covalently linked to the GQDs in DMSO are shown in Fig. 4b. The absorption maximum (Q band) for the **Pc** was observed at 691 nm, while there is up to 5 nm shift to lower wavelengths for phthalocyanine-GQDs nanocomposites, Table 1. Also, there is noticeable strong absorption in the B band region for the phthalocyanine-GQDs nanocomposites compared to the free phthalocyanine, this corresponds to the region where the GQDs absorb.

XPS Spectra

X-ray photoelectron spectroscopy (XPS) was used to confirm the elemental compositions of GQDs, NGQDs and SNGQDs before and after covalent bonding to **Pc**, Fig. 5. The full survey scans of all the GQDs show expected atoms with NGQDs and SNGQDs showing addition of N, and N, S atoms,

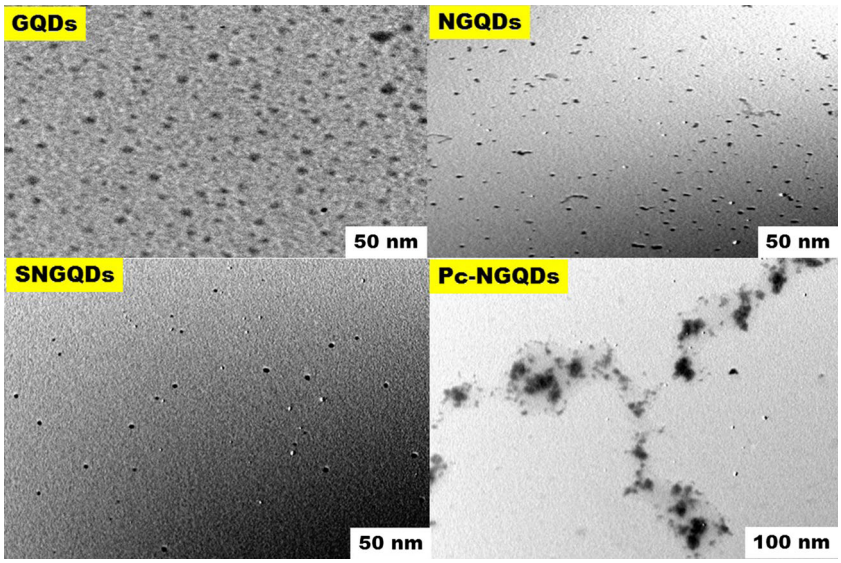

Fig. 3 TEM images of pristine GQDs, NGQDs, SNGQDs and **Pc**-NGQDs

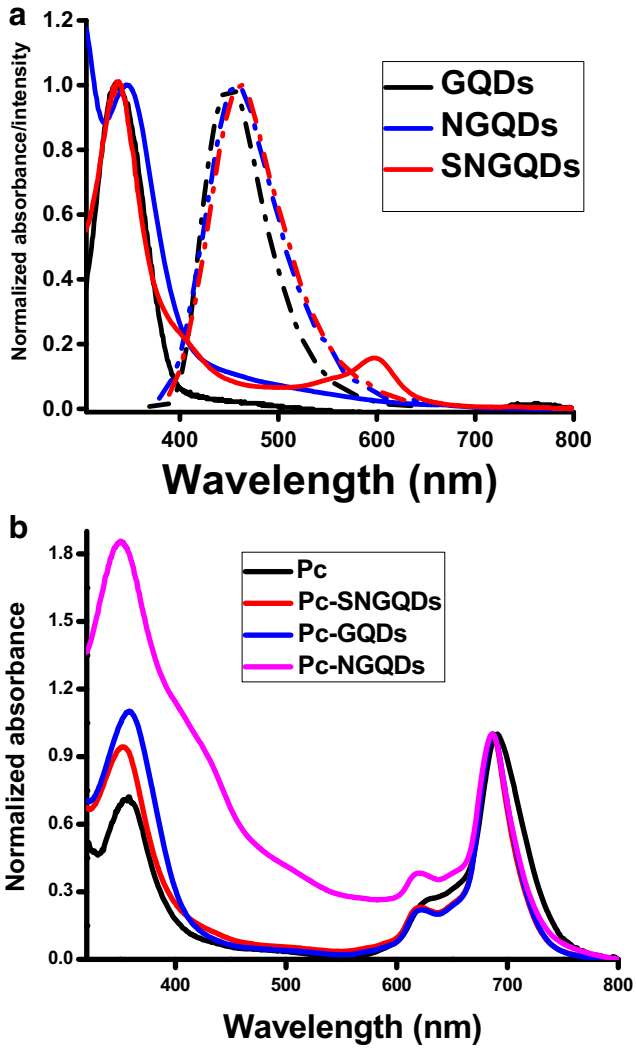

Fig. 4 (**a**) Absorption (*solid lines*) and emission (*dash dot lines*) spectra of GQDs, NGQDs, and SNGQDs in water and (**b**) Absorption spectra of **Pc, Pc**-SNGQDs**, Pc**-GQDs and **Pc**-NGQDs. composites in DMSO

respectively which are not present in pristine GQDs. The presence of Na auger peak at 298 eV in the XPS spectrum of GQDs is due to the NaOH used during its preparation. No other contaminating element(s) was detected in the XPS spectral of the QDs.

The survey scans of **Pc**-QDs (using **Pc-**SNGQDs as example) showed the peaks due to C1s, S (2p and S 2 s), N1s, and O1s, appearing along with Zn ($2p_{3/2}$ and Zn $2p_{1/2}$) in their respective peak positions. The presence of Zn in the spectral of **Pc**-QDs confirms the presence of the **Pc** and QDs.

Figure 6a shows the N1s spectrum of **Pc** which was deconvoluted into two chemically distinct peak positions at 398.81 eV and 400.97 eV, these peaks correspond to N–C (from **Pc** ring) and N–H (from NH_2), respectively. Three distinct peaks corresponding to N–C, N–H and N–C = O were deconvoluted for the N1s of **Pc-**GQDs at 399.94, 401.12 and 402.13 eV, respectively. The latter confirming the presence of the amide bond. N1s spectral of **Pc-**SNGQDs was deconvoluted to reveal the presence of pyridinic N, N-C/ pyrrolic N, N-H and N–C = O at 399.25, 400.08, 401.06 and 401.97 eV, respectively. The deconvolution of N1s spectrum of **Pc**-NGQDs gave similar peaks to those of **Pc-**SNGQDs, except that the N–C = O (due to amide bonding) shifted to higher binding energy at 403.10 eV. Pyridinic N and pyrrolic N peaks are due to the doping of graphene QDs with N-containing molecules [8, 36].

Photophysical Studies

The fluorescence quantum yields and lifetimes for the QDs, **Pc** and the conjugates are summarized in Table 1. The $\Phi_{F(QDs)}$ (where GQDs absorb) for GQDs, NGQDs and SNGQDs have been reported before [21]. The fluorescence quantum yields ($\Phi_{F(QDs)}$) of the conjugates at the wavelengths where QDs

Table 1 Photophysical parameters of graphene quantum dots, Pc and the conjugates recorded in DMSO

Sample	λ_{abs} [b,c] (nm)	$\Phi_{F(Pc)}$ [d]	$\Phi_{F(QDs)}$ [c,e]	$\tau_{F(Pc)}$ (ns)[d]	$\tau_{F(QDs)}$ [c,e] (ns)	τ_T (μs)	Φ_T	FRET Eff
Pc[a]	691	0.18	–	2.73	–	240	0.73	–
Pc-GQDs	686 (334)	0.25	0.10 (0.21)	2.89	5.17 (5.7)	194	0.74	0.52
Pc-NGQDs	687 (341)	0.23	0.31 (0.77)	2.86	6.811 (7.8)	205	0.77	0.59
Pc-SNGQDs	687 (337)	0.20	0.31 (0.81)	2.84	3.96 (11.6)	187	0.79	0.61

[a] Values from Ref. [23]

[b] λ_{abs} = absorption wavelength

[c] values in brackets are for QDs alone in water

[d] Excitation where Pc absorbs

[e] Excitation where QDs absorb, values for GQDs alone are from reference [21]

absorb were found to be up to 2.6 times lower than the GQDs alone. The decrease is due to Förster resonance energy transfer (FRET) and other energy transfer processes which has been reported to deactivate the emission of the QDs [37, 38].

FRET efficiency for the conjugates were determined from the fluorescence quantum yields of the conjugates and unconjugated QDs at excitation wavelength where QDs absorb, Eq. 8, [39]. The calculated FRET Eff ranged from 0.52 to 0.61, Table 1.

$$\text{Eff} = 1 - \frac{\Phi_{F(Pc-QDs)}}{\Phi_{F(QDs)}} \tag{8}$$

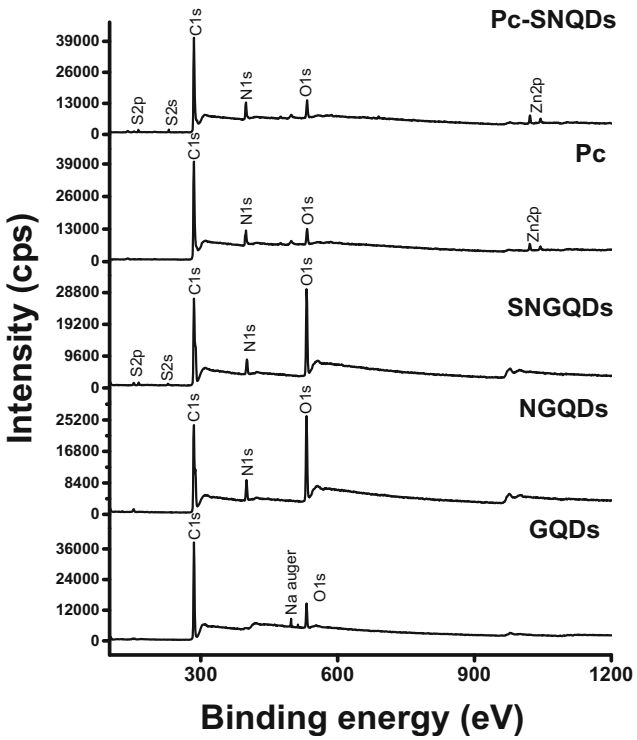

Fig. 5 X-ray photoelectron (XPS) wide-scan spectra of GQDs, NGQDs, SNGQDs, **Pc**, and **Pc**-SNGQDs

The highest FRET efficiency was obtained for SNGQDs due to the more red shifted emission spectrum and slightly more overlap with **Pc** absorption, Fig. 7.

The $\Phi_{F(Pc)}$ of the **Pc**-QDs at the excitation wavelength of 613 nm where only **Pc** absorbs are larger than the unconjugated **Pc**. Reduction in Φ_F are mostly reported for metal-based nanomaterials when conjugated to phthalocyanines due to heavy atom effects of the nanoparticles. However, we observe an increase in Table 1. Increases in Φ_F for **Pc** covalently linked to QDs and magnetic nanoparticles have been reported, and attributed to the nature or the length of the spacer [40]. Fluorescence lifetimes (τ_F) were obtained from TCSPC technique by fitting the fluorescence decay data to a mono-exponential function for all the conjugates. The increase in the $\Phi_{F(Pc)}$ values were complemented by increase in the fluorescence lifetimes ($\tau_{F(Pc)}$) for the conjugates measured at the excitation wavelengths of the **Pc**. Similarly, at the excitation wavelengths where the QDs absorb, the fluorescence lifetimes ($\tau_{F(QDs)}$) of the conjugates were observed to be significantly short-lived compared to the lifetimes of the QDs (in brackets) alone, corresponding to decrease in quantum yields.

The triplet quantum yields absorption (Φ_T) and lifetimes recorded in DMSO at 675 nm cross-over wavelength are summarized in Table 1. The measured triplet quantum yields (Φ_T) of the samples are 0.73, 0.74, 0.77 and 0.79 for **Pc**, **Pc**-GQDs, **Pc**-NGQDs and **Pc**-SNGQDs, respectively. The value for pristine GQDs is almost the same as for the Pc alone. Slight increases for **Pc**-NGQDs and **Pc**-SNGQDs could be due to the presence of heteroatoms. The presence of sulphur as opposed to oxygen bridges is also known [41] to improve intersystem crossing to the triplet state of the phthalocyanine. In addition, the slight increase in Φ_T could be ascribed to the large conjugative systems of graphene QDs which significantly reduced the singlet-triplet splitting and thus enhance the probability of intersystem crossing [42].

Triplet lifetimes of the samples were determined by exponential fitting of the kinetic curves (**Pc**-SNGQDs as

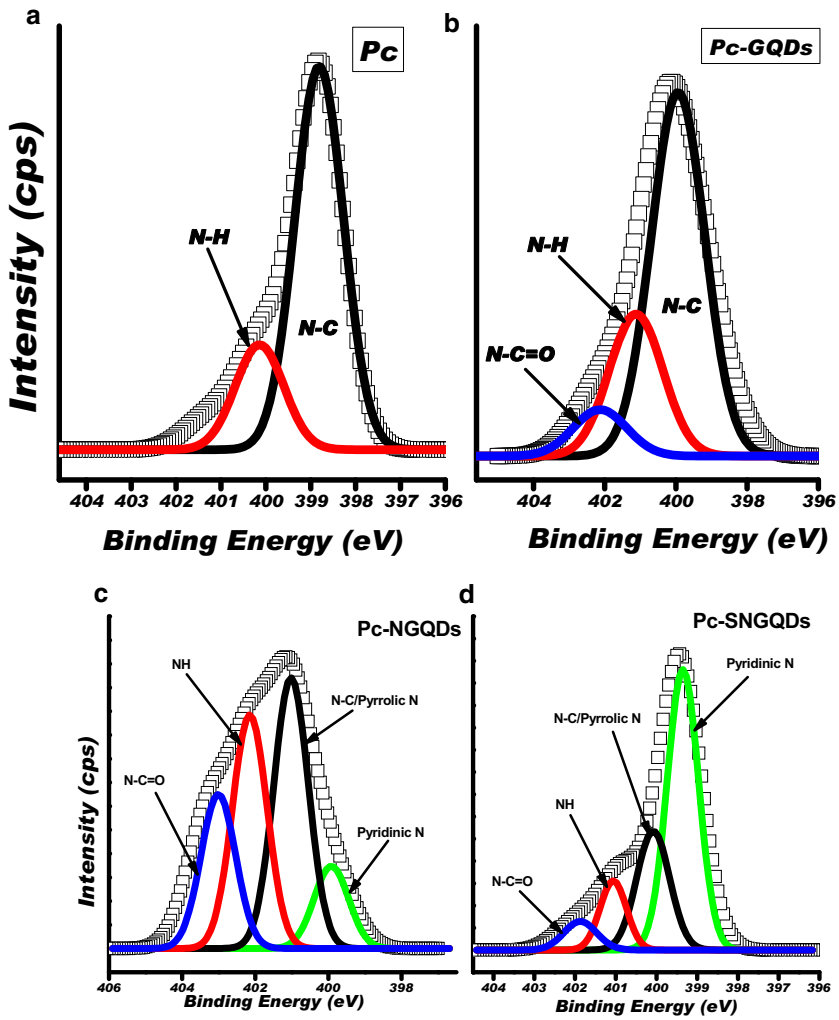

Fig. 6 High resolution of deconvoluted N1s XPS spectra for (**a**) **Pc**, (**b**) **Pc**-GQDs (**c**) **Pc**-NGQDs, and (**d**) **Pc**-SNGQDs

representative) using OriginPro 2016 in Fig. 8. Table 1 shows that the triplet lifetimes for the **Pc** and its conjugates ranged from 187 to 240 μs. The longest triplet lifetime of **Pc** at 240 μs is consistent for a molecule with smallest triplet quantum yield to have longest lifetime [43], and vice versa.

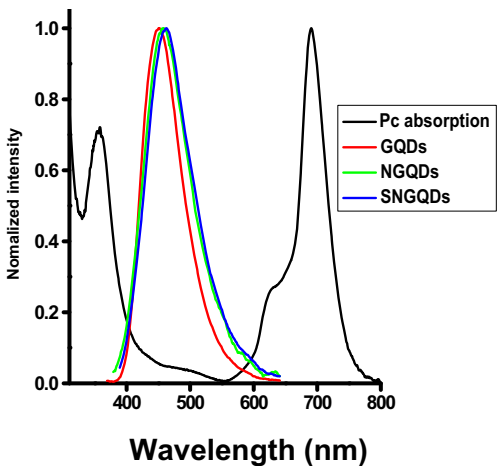

Fig. 7 Absorption spectrum of **Pc** (in DMSO) and emission spectra of GQDs, NGQDs and SNGQDs in water (λ_{exc} = 330–370 nm)

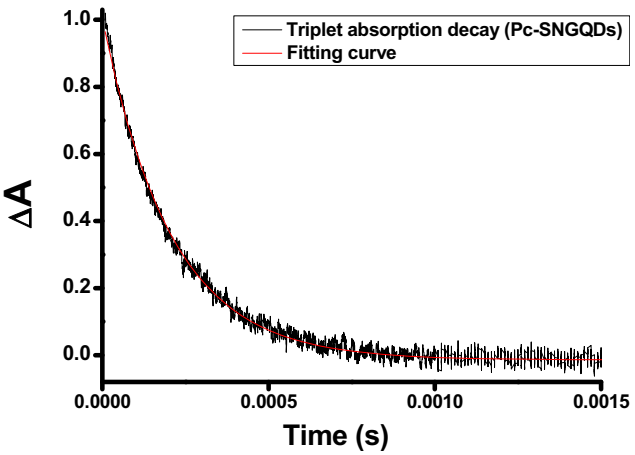

Fig. 8 Triplet absorption decay curve of **Pc**-SNGQDs with exponential fitting curve in red

Nonlinear Optical (NLO) Studies

Z Scan Profiles

Figure 9a shows the overlay of open aperture Z-scan profiles for the studied samples measured in DMSO at 2 absorbance for each sample. The samples were all excited at 532 nm wavelength and 10 ns (FWHM) duration using a mode-locked Nd:YAG laser beam. At constant irradiance intensity of ca. 0.08 GW/cm^2, the transmittance decreased along the sample positions (z) relative to the focal point (z = 0).

The reduction in the transmitted beam with increasing optical input intensity is an indication of positive nonlinear absorption [28, 30, 44], and presence of reverse saturable absorbers [45–48].

The magnitude of nonlinear optical effects induced as a result of laser light-matter interactions were evaluated in terms of nonlinear absorption coefficient (β_{eff}) by fitting theoretical datasets using Eq. 4 to experimental datasets as shown in Fig. 9b. The β_{eff} values for **Pc**, **Pc**-GQDs, **Pc**-NGQDs and **Pc**-SNGQDs are 225.4 cm/GW, 231.0 cm/GW, 287.6 cm/GW and 319.8 cm/GW, respectively, Table 2. There was a large increase in β_{eff} values for **Pc**-NGQDs and **Pc**-SNGQDs

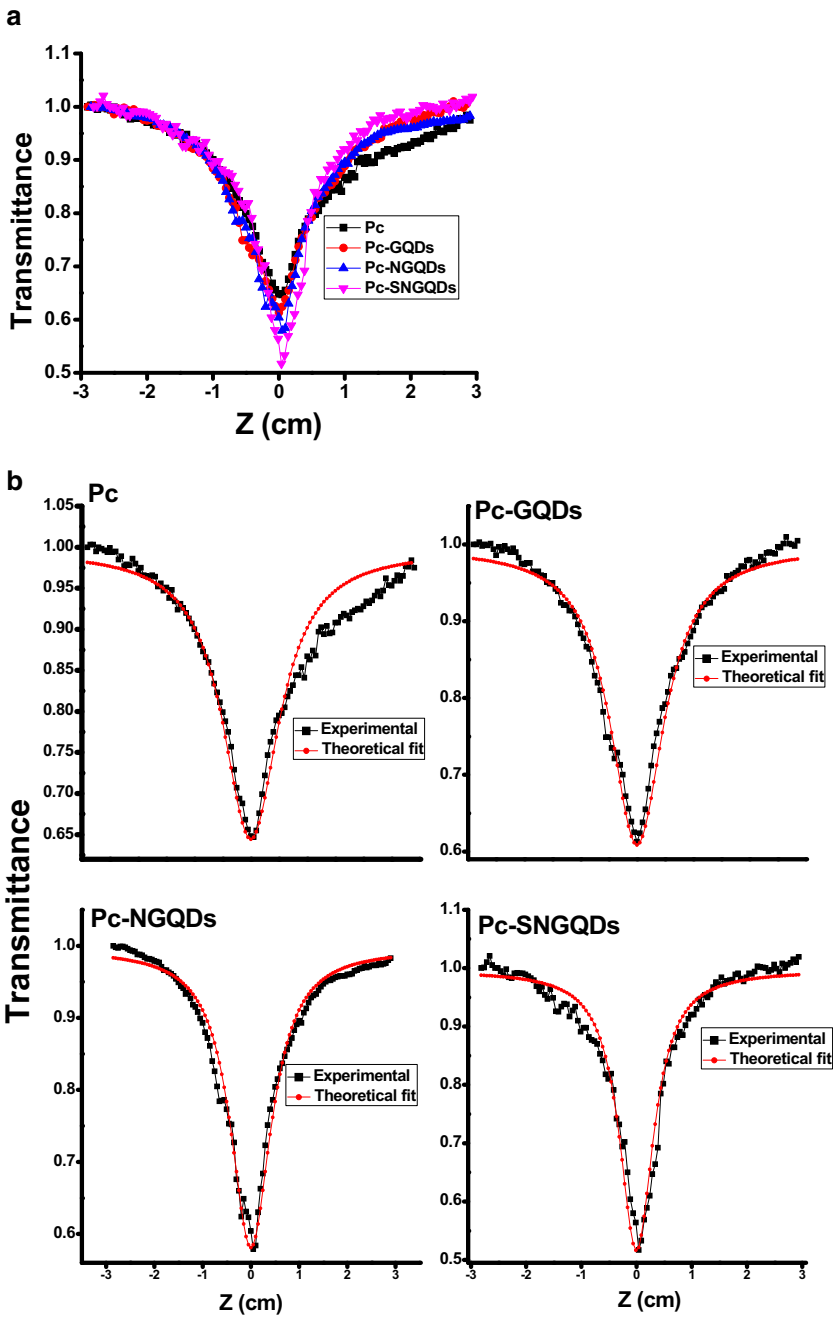

Fig. 9 (**a**) Open Aperture Z-scan signatures of the **Pc** and **Pc**-GQDs conjugates and (**b**) Plots showing fitting of theoretical data (*red*) to experimental data (*black*) for **Pc**, **Pc**-GQDs, **Pc**-NGQDs and **Pc**-SNGQDs for evaluating β_{eff}. Absorbance = 2.0, $I_{00} \approx 0.08$ GW/cm^2 for each independent measurement

Table 2 Nonlinear optical properties of the Pc and Pc-GQDs conjugates in DMSO at 532 nm excitation wavelength and 10 ns pulses

Sample	β_{eff} (cm/GW)	$I_m[\chi^{(3)}]$ (esu)	γ (esu)	I_{lim} (J/cm^2)
Pc	225.4	8.73×10^{-11}	4.22×10^{-29}	0.77
Pc-GQDs	231.0	9.16×10^{-11}	7.01×10^{-29}	0.61
Pc-NGQDs	287.6	1.32×10^{-10}	3.34×10^{-28}	0.58
Pc-SNGQDs	319.8	3.42×10^{-10}	5.03×10^{-28}	0.55

compared to **Pc** and **Pc**-GQDs. The significant increase in the nonlinear absorption by **Pc** when conjugated to NGQDs or SNGQDs could be as a result of increase in triplet absorption populations (increased triplet quantum yields) which could generate substantial NLO effect of reverse saturable absorption (RSA) [48–51] compared to **Pc** and **Pc**-GQDs as seen in Fig. 9a.

Bourlinos and co-workers reported on significantly enhanced nonlinear absorption for boron doped carbon dots compared to un-doped carbon dots at 532 nm, using 35 ps and 4 ns laser pulses [13]. Similarly, doping of quantum dots (graphene quantum dots inclusive) with heteroatoms can endow the QDs with new or improved electronic states [8, 52, 53], photophysical and photoluminescence properties [6, 8, 54–56]. Hence, improved nonlinear absorption (NLA) of **Pc**-NGQDs and **Pc**-SNGQDs could be due to the improved photophysical properties and formation of new electronic states that could lead to enhanced nonlinear absorptions [14].

Nonlinear Optical Parameters

The imaginary third-order susceptibility, $I_m[\chi^{(3)}]$, and second-order hyperpolarizability, γ, measured in esu, were evaluated as a function of β_{eff} using Eqs. 6 and 7, respectively. A good OL device should possess high absorbency to effectively limit incident laser radiation. Therefore, a molecular material with relatively high γ and/or $I_m[\chi^{(3)}]$ values can be used for designing OL devices to protect light sensitive materials and to enhance night vision against intense laser radiation. The values of γ and $I_m[\chi^{(3)}]$ are expected to follow the same trend as observed for β_{eff}. From Table 2, the $I_m[\chi^{(3)}]$ value of **Pc** and **Pc**-GQDs are within the same range and up to one order of magnitude lower than the values for **Pc**-NGQDs and **Pc**-SNGQDs**.** Similar trends were also observed for values reported for γ. Larger values of **Pc**-NGQDs and **Pc**-SNGQDs could be attributed to the surface defects introduced on the graphene quantum dots after doping with S and/or N [8, 10, 36]. The $I_m[\chi^{(3)}]$ value of $17.62 \pm 4.03 \times 10^{-12}$ esu in DMF at 532 nm and 6 ns pulses [18] reported for similar **Pc** covalently linked to GO is up to 1 or 2 order of magnitude lower than the values reported for **Pc**-QDs conjugates in this work. The remarkably improved NLA for our molecules can

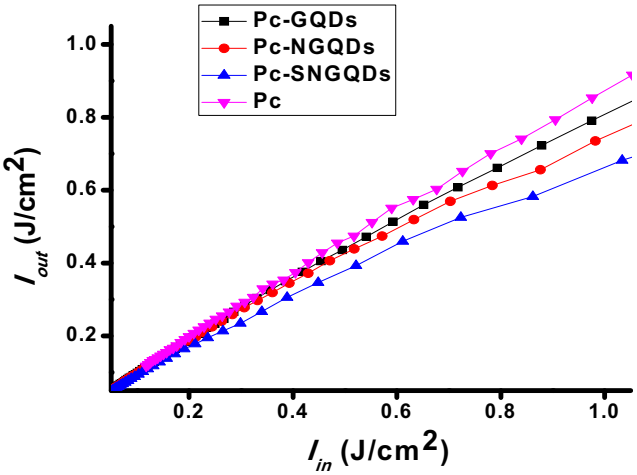

Fig. 10 Output fluence (I_{out}) versus input fluence (I_o) for **Pc, Pc**-GQDs, **Pc**-NGQDs and **Pc**-SNGQDs. Peak intensity (I_{00}) ≈ 0.08 GW cm^{-2} for each sample

be ascribed to enhanced quantum confinement effect and the edge effects of graphene quantum dots compared to bulk graphene oxide [57, 58]. Also, differences from solvent polarities, Z-scan experimental conditions and procedures cannot be ruled out.

Incident intensity threshold, (I_{lim}), is a measure of deviation of energy output by OL devices from incident laser light. Therefore, the larger the deviation from incident laser light (that is, lower I_{lim}), the better the material as optical limiter. Figure 10 shows the plots of incident laser intensity (I_{in}) versus transmitted laser intensity (I_{out}) for **Pc** and **Pc**-GQDs conjugates at input intensity of 0.08 GW cm^{-2}. Both the conjugates and **Pc** have their energy outputs expectedly deviated from linearity, an indicative of better and good NLO responses to the input intensity [59]. However, energy outputs of **Pc** conjugated to NGQDs and SNGQDs were substantially lower compared to **Pc** and **Pc**-GQDs. From Table 2, the I_{lim} values for **Pc**, **Pc**-GQDs **Pc**-NGQDs and **Pc**-SNGQDs in DMSO were estimated at 0.77 J/cm^2, 0.61 J/cm^2, 0.58 J/cm^2 and 0.55 J/cm^2, respectively.

Conclusion

The pristine graphene (GQDs), nitrogen-doped (NGQDs) and sulfur-nitrogen co-doped (SNGQDs) graphene quantum dots were covalently linked to mono-amino zinc phthalocyanine and the characterizations were in good agreements with the expected results. The conjugates were also subjected to open aperture Z-scan measurements to monitor their behaviour under tightly focussed Gaussian laser beam. The magnitude of nonlinear interactions between the samples and the laser were quantified in form of nonlinear absorption coefficient. Nonlinear effect due to reverse saturable absorption was the predominant mechanism; and it was attributed to the

moderately enhanced triple population. The major factor responsible for the enhanced nonlinearities in the **Pc**-NGQDs and **Pc**-SNGQDs were fully described and attributed to the surface defects caused by the presence of heteroatoms such as nitrogen and sulphur.

Acknowledgements This work was supported by the Department of Science and Technology (DST)/Nanotechnology (NIC) and National Research Foundation (NRF) of South Africa through DST/NRF South African Research Chairs Initiative for Professor of Medicinal Chemistry and Nanotechnology (UID 62620) and Rhodes University.

Compliance with Ethical Standards There are no potential conflicts of interest with regard to this manuscript. The funders have agreed to publication. The research does not involve human participants and/or Animals.

References

1. Li Y, Shu H, Wang S, Wang J (2015) Electronic and optical properties of graphene quantum dots: The role of many-body effects. J Phys Chem C 119:4983–4989
2. Yamijala SSRKC, Mukhopadhyay M, Pati SK (2015) Linear and nonlinear optical properties of graphene quantum dots: A computational study. J Phys Chem C 119:12079–12087
3. Lee MW, Kim J, Suh JS (2015) Characteristics of graphene quantum dots determined by edge structures: three kinds of dots fabricated using thermal plasma jet. RSC Adv 5:67669–67675
4. Liu Y, Wu P (2013) Graphene quantum dot hybrids as efficient metal-free electrocatalyst for the oxygen reduction reaction. ACS Appl Mater Interfaces 5:3362–3369
5. Luk CM, Tang LB, Zhang WF, Yu SF, Teng KS, Lau SP (2012) An efficient and stable fluorescent graphene quantum dot-agar composite as a converting material in white light emitting diodes. J Mater Chem 22:22378–22381
6. Liu Q, Guo B, Rao Z, Zhang B, Gong JR (2013) Strong two photon-induced fluorescence from photostable, biocompatible nitrogen-doped graphene quantum qots for cellular and deep-tissue imaging. Nano Lett 13:2436–2441
7. Li Y, Zhao Y, Cheng H, Hu Y, Shi G, Dai L, Qu L (2012) Nitrogen-doped graphene quantum dots with oxygen-rich functional groups. J Am Chem Soc 134:15–18
8. Qu D, Zheng M, Du P, Zhou Y, Zhang L, Li D, Tan H, Zhao Z, Xied Z, Sun Z (2013) Highly luminescent S, N co-doped graphene quantum dots with broad visible absorption bands for visible light photocatalysts. Nanoscale 5:12272–12277
9. Qu LT, Liu Y, Baek JB, Dai LM (2010) Nitrogen-doped graphene as efficient metal-free electrocatalyst for oxygen reduction in fuel Cells. ACS Nano 4:1321–1326
10. Qu D, Sun Z, Zheng M, Li J, Zhang Y, Zhang G, Zhao H, Liu X, Xie Z (2015) Three colors emission from S, N co-doped graphene quantum dots for visible light H_2 production and bioimaging. Adv Op Mater 3:360–367
11. Liu Y, Park HG, Lee JH, Seo DS, Kim EM, Heo GS (2015) Electro-optical switching of liquid crystals sandwiched between ion-beam-spurted graphene quantum dots-doped PEDOT:PSS composite layers. Opt Express 23:34071–34081
12. Cho MJ, Park HG, Jeong HC, Lee JW, Jung YH, Kim DH, Kim JH, Lee JW, Seo DS (2014) Superior fast switching of liquid crystal devices using graphene quantum dots. Liq Cryst 14:761–767
13. Bourlinos AB, Trivizas G, Karakassides MA, Baikousi M, Kouloumpis A, Gournis D, Bakandritsos A, Hola K, Kozak O, Zboril R, Papagiannnouli I, Aloukos P, Couris S (2015) Green and simple route toward boron doped carbon dots with significantly enhanced non-linear optical properties. CARBON 83:173–179
14. Imakita K, Ito M, Fujii M, Hayashi S (2009) Ultrafast third order properties of phosphorus-doped Si nanocrystals embedded in phosphosilicate glass thin films. Opt Express 17:7368–7376
15. Kanbara H, Maruno T, Yamashita A, Matsumoto S, Hayashi T, Konami H, Tanaka N (1996) Third-order nonlinear optical properties of phthalocyanine and fullerene. J Appl Phys 80:3674
16. Wang J, Blau WJ (2008) Linear and nonlinear spectroscopic studies of phthalocyanine-carbon nanotube blends. Chem Phys Lett 465: 265–271
17. Sanusi K, Amuhaya EK, Nyokong T (2014) Enhanced optical limiting behavior of an indium phthalocyanine − single-walled carbon nanotube nomposite: an investigation of the effects of solvents. J Phys Chem C 118:7057–7069
18. Zhu J, Li Y, Chen Y, Wang J, Zhang B, Zhang J, Blau WJ (2011) Graphene oxide covalently functionalized with zinc phthalocyanine for broadband optical limiting. CARBON 49:1900–1905
19. Yu X, Zhan C, Huang Y (2012) Synthesis and characterization of new asymmetrical phthalocyanine zinc. Chin J Org Chem 32:770–775
20. Kudrevich SV, Ali H, van Lier JE (1994) Syntheses of monosulfonated phthalocyanines, benzonaphthoporphyrazines and porphyrins via the Meerwein reaction. J Chem Soc Perkin Trans 1:2767–2774
21. Achadu OJ, Nyokong T (2016) Interaction of graphene quantum dots with 4-acetamido-2,2,6,6-tetramethylpiperidine-oxyl free radicals: A spectroscopic and fluorimetric study. J Fluoresc 26:283–295
22. Fashina A, Antunes E, Nyokong T (2013) Characterization and photophysical behavior of phthalocyanines when grafted onto silica nanoparticles. Polyhedron 53:278–285
23. Bankole OM, Nyokong T (2016) Nonlinear optical response of a low symmetry phthalocyanine in the presence of gold nanoparticles when in solution or embedded in poly acrylic acid polymer thin films. J Photochem Photobiol A Chem 319–320:8–17
24. Ogunsipe A, Chen JY, Nyokong T (2004) Photophysical and photochemical studies of zinc(II) phthalocyanine derivatives-effects of substituents and solvents. New J Chem 7:822–827
25. Tran-Thi TH, Desforge C, Thiec C, Gaspard S (1989) Singlet-singlet and triplettriplet intramolecular transfer processesin a covalently linked porphyrin-phthalocyanine heterodimer. J Phys Chem 93:1226–1233
26. Fery-Forgues S, Lavabre D (1999) Are fluorescence quantum yields so tricky to measure? A demonstration using familiar stationery products. J Chem Educ 76:1260–1264
27. Kubat P, Mosinger J (1996) Photophysical properties of metal complexes of mesotetrakis(4-sulphonatophenyl) porphyrin. J Photochem Photobiol A 96:93–97
28. Sheik-Bahae M, Said AA, Wei TH, Hagan DJ, Van Stryland EW (1990) Sensitive measurement of optical nonlinearities using a single beam. IEEE J Quantum Electron 26:760–769
29. Van Stryland EW, Sheik-Bahae M (1998) In: Kuzyk MG, Dirk CW (eds) Characterization techniques and tabulations for organic nonlinear materials. Marcel Dekker, Inc, New York, pp 655–692
30. Kumar RSS, Rao SV, Giribabu L, Rao DN (2007) Femtosecond and nanosecond nonlinear optical properties of alkyl phthalocyanines studied using Z-scan technique. Chem Phys Lett 447:274–278
31. Dini D, Hanack M (2003) In: Kadish KM, Smith KM, Guilard R (eds) The porphyrin handbook: physical properties of phthalocyanine-based materials, 17. Academic Press, USA, p 2
32. Pan D, Zhang J, Li Z, Wu M (2010) Hydrothermal route for cutting graphene sheets into blue-luminescent graphene quantum dots. Adv Mater 22:734–738

33. Tang L, Ji R, Cao X, Lin J, Jiang H, Li X, Teng KS, Luk CM, Zeng S, Hao J, Lau SP (2012) Deep ultraviolet photoluminescence of water-soluble self-passivated graphene quantum dots. ACS Nano 6:5102–5110
34. Achar BN, Lokesh KS (2004) Studies on phthalocyanine sheet polymers. J Organomet Chem 689:2601–2605
35. Zheng XT, Ananthanarayanan KQ, Luo P, Chen P (2015) Glowing graphene quantum dots and carbon dots: properties, syntheses, and biological applications. Small 11:1620–1636
36. Qu D, Zheng M, Zhang L, Zhao H, Xie Z, Jing X, Raid EH, Fan H, Sun Z (2014) Formation mechanism and optimization of highly luminescent N-doped graphene quantum dots. Sci Rep 4:5294–5303
37. Zenkevich EI, Stupak AP, Kowerko D, Von Borczyskowski C (2012) Influence of single dye molecules on temperature and time dependent optical properties of CdSe/ZnS quantum dots: Ensemble and single nanoassembly detection. Chem Phys 406:21–29
38. Blaudeck T, Zenkevich EI, Cichos F, Von Borczyskowski C (2008) Probing wave functions at semiconductor quantum-dot surfaces by non-FRET photoluminescence quenching. J Phys Chem C 112: 20251–20257
39. Lakowicz JR (2009) Principles of Fluorescence Spectroscopy, 3rd edn. Springer, New York, p 243
40. Corr SA, Byrne AO', Gun'ko YK, Ghosh S, Brougham DF, Mitchell S, Volkov Y, Prina-Mello A (2006) Magnetic-fluorescent nanocomposites for biomedical multitasking. Chem Commun 4474–4476. doi:10.1039/B610746J
41. Galstyan A, Riehemann K, Schäfers M, Faust A (2016) A combined experimental and computational study of the substituent effect on the photodynamic efficacy of amphiphilic Zn(II)phthalocyanines. J Mater Chem B 4:5683–5691
42. Englman R, Jortner J (1970) The energy gap law for non-radiative decay in large molecules. J Lumin 12:134–142
43. Darwent JR, Douglas P, Harriman A, Porter G, Richoux MC (1982) Metal phthalocyanines and porphyrin for reduction of water to hydrogen. Coord Chem Rev 44:83–126
44. Sheik-Bahae M, Said AA, Stryland EW (1989) High-sensitivity, single-beam n2 measurements. Opt Lett 14:955–957
45. Dini D, Yang GY, Hanack M (2003) Perfluorinated phthalocyanines for optical limiting: evidence for the direct correlation between substituent electron withdrawing character and the nonlinear optical effect. J Chem Phys 119:4857–4864
46. de la Torre G, Vázquez P, Agulló-López F, Torres T (2004) Role of structural factors in the nonlinear optical properties of phthalocyanines and related compounds. Chem Rev 104:3723–3750
47. Sutherland RL (2003) In handbook of nonlinear optics, 2nd edn. Marcel Dekker, New York, **Revised and expanded**
48. Shirk JS, Flom SR, Pong RGS, Heckmann H, Hanack M (2000) Effect of axial substitution on the optical limiting properties of indium phthalocyanines. J Phys Chem 104:1438–1449
49. Blau W, Byrne H, Dennis WM, Kelly JM (1985) Reverse saturable absorption in tetraphenylporphyrins. Opt Commun 56:25–29
50. Shirk JS, Flom SR, Lindle JR, Bartoli FJ, Snow AW, Boyle ME (1994) Nonunear Absorption in Phthalocyanines and Naphthalocyanines. MRS Symp Proc 328:661–666
51. Perry JW, Mansour K, Lee IYS, Wu XL, Bedworth PV, Chen CT, Marder SR, Ng D, Miles P, Wada T, Tian M, Sasabe H (1996) Organic optical limiter with a strong nonlinear absorptive response. Science 273:1533–1536
52. Gu J, Zhang X, Pang A, Yang J (2016) Facile synthesis and photoluminescence characteristics of blue-emitting nitrogen-doped graphene quantum dots. Nanotechnology 27:165704
53. Li X, Lau SP, Tang L, Ji R, Yang P (2014) Sulphur doping: a facile approach to tune the electronic structure and optical properties of graphene quantum dots. Nanoscale 6:5323–5328
54. Cao L, Meziani MJ, Sahu S, Sun YP (2012) Photoluminescence properties of graphene versus other carbon nanomaterials. Acc Chem Res 46:171–180
55. Liu S, Tian J, Wang L, Zhang Y, Qin X, Luo Y, Asiri AM, Al-Youbi AO, Sun X (2012) Hydrothermal treatment of grass: A low-cost, green route to nitrogen-doped, carbon-rich, photoluminescent polymer nanodots as an effective fluorescent sensing platform for label-free detection of Cu(II) ions. Adv Mater 24:2037–2041
56. Wang Y, Shao Y, Matson DW, Li J, Lin Y (2010) Nitrogen-doped graphene and its application in electrochemical biosensing. ACS Nano 4:1790–1798
57. Zhang F, Liu F, Wang C, Xin X, Liu J, Guo S, Zhang J (2016) Effect of lateral size of graphene quantum dots on their properties and application. ACS Appl Mater Interfaces 8:2104–2110
58. Hassan M, Haque E, Reddy KR, Minett AI, Chenc J, Gomes VG (2014) Edge-enriched graphene quantum dots for enhanced photoluminescence and supercapacitance. Nanoscale 6:11988–11994
59. Dini D, Vagin S, Hanack M, Amendola V, Meneghetti M (2005) Nonlinear optical effects related to saturable and reverse saturable absorption by subphthalocyanines at 532 nm. Chem Commun 3796–3798. doi:10.1039/B502359A